Impedance Control Strategies for Lower-Limb Exoskeletons

8

Luis Arciniegas-Mayag, Carlos Rodriguez-Guerrero, Eduardo Rocon, Marcela Múnera, and Carlos A. Cifuentes

8.1 Introduction

A user who has suffered a stroke usually has several limitations in the motor control of his or her limbs. In general terms, the quality of life of users and other dependency-related factors are affected. For example, daily living activities comprise some tasks that the user's efficiency has decreased. These activities are defined as the fundamental processes that allow humans to have a high independence level in daily life. Examples of them are feeding, dressing, and actions related to personal hygiene [1, 2]. The activities of daily living are classified according to their complexity into basic and instrumental. Basic activities are related to self-care and personal mobility [3] and include cleaning, eating, and physical exercise. The instrumental activities of daily living require a higher cognitive level development [2–4]. Examples are buying, preparing food, cleaning, maintaining the house, among others. However, both types depend on mobility, which is deeply affected in patients who suffer a stroke. Some activities such as sitting/standing, ascending, and descending stairs are related to mobility and the user change of position [5]. In a particular case, the walking activity has been included in these tasks that provide the

L. Arciniegas-Mayag · M. Múnera · C. A. Cifuentes (✉)
Biomedical Engineering, Department of the Colombian School of Engineering Julio Garavito, Bogotá D.C., Colombia
e-mail: luis.arciniegas@mail.escuelaing.edu.co; marcela.munera@escuelaing.edu.co; carlos.cifuentes@escuelaing.edu.co

C. Rodriguez-Guerrero
Robotics & Multibody Mechanics Research Group, Department of Mechanical Engineering, Vrije Universiteit Brussel, Elsene, Belgium
e-mail: carlos.rodriguez.guerrero@vub.be

E. Rocon
Centro de Automática y Robótica, CSIC-UPM, Arganda del Rey, Madrid, Spain
e-mail: e.rocon@csic.es

C. A. Cifuentes, M. Múnera, *Interfacing Humans and Robots for Gait Assistance and Rehabilitation*, https://doi.org/10.1007/978-3-030-79630-3_8

user's mobility and improve quality of life (QoL). For this reason, different session therapies have been designed for the recovery of this activity in users that suffered a stroke [6]. Subsequently, the development of these therapy sessions represents a high workload for the post-stroke user and the physiotherapist [7, 8]. Additionally, it represents a heavy burden of the disease on the user [9, 10]. In this sense, in the last decades, various alternatives have been proposed to improve the effectiveness of therapy sessions focused on improving the gait pattern in post-stroke users. One of the options has been the use of a wearable robots, in this case, the development and implementation of lower-limb exoskeletons [11] used to recover the primary movements of the user's lower limbs retraining the user in the walking activity.

As mentioned in Chap. 1, the lower-limb exoskeletons have been implemented in different workspaces. This wearable robot has been focused on three objectives: Power augmentation, assistance, and rehabilitation, where each one is targeted to a different population. Each one of these objectives is related to some aspects that define a lower-limb exoskeleton. Therefore, it is defined some control strategies according to the activities of daily living that the lower-limb exoskeletons complement the human body's primary movements.

This chapter presents the development and implementation of two control strategies based on the principle of impedance. The control is explained through the Human–Robot interface of the *AGoRA* exoskeleton (Colombian school of engineering Julio Garavito, Colombia) and a case study is presented for the controllers.

8.2 Human–Robot Interaction

In the definition of (HRI), it is mandatory to determine some parameters of the human used as an input to a wearable robot. In this concept, an initial stage called cognitive process is developed, defined some phases that a human executes for the development of an activity. The user's movements are divided into three steps: a reasoning phase, a planning phase, and the executing phase [12]. As a result, the lower-limb's movements are generated to execute activities of daily living. Currently, the cognitive process development is estimated using a cognitive human–robot interaction (cHRI). As a result, a connection is created between the user and the wearable robot for the acquisition and of these cognitive processes. For this purpose, brain-machine interfaces (BCI) or human–machine interfaces (HMI) are used. The development of these interfaces uses various alternatives to acquire signals from the human body. As an example, interfaces are used for the acquisition of Electroencephalographic (EEG) signals [13–15] and electromyography (EMG) signals [16–18] adapted to the sensory interface of a wearable robot. Thus, using these signals an alternative for estimating the user's cognitive processes was implemented. the process of pHRI generation is shown in Fig. 8.1

EEG and EMG signals were implemented to estimate cHRI in the control strategies development based on user-generated parameters. On the other hand, these signals require the user's instrumentation on various parts of the body. For

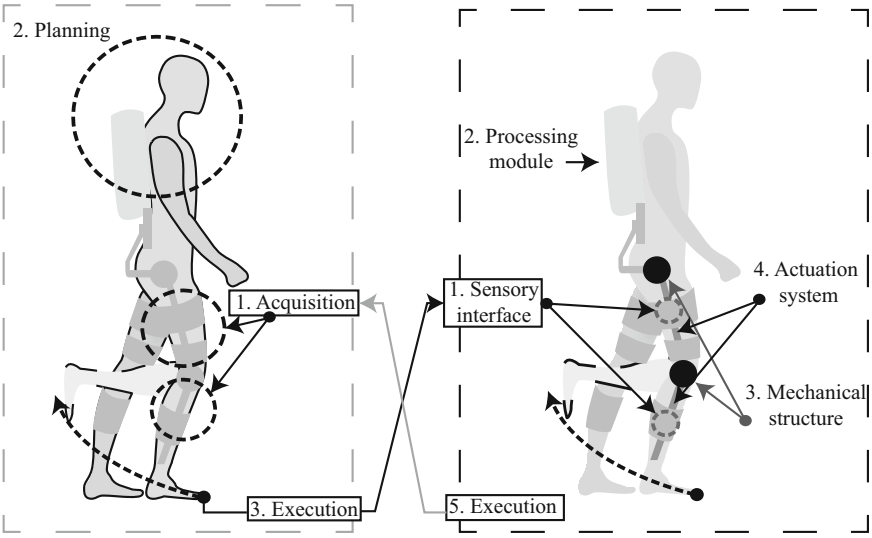

Fig. 8.1 pHRI definition using lower-limb exoskeleton in users that suffer a neurological pathology that affects the lower-limb's motor control; (**a**) shows the lower-limb movement generation through the Acquisition, planning, and lower-limb movement execution phases, respectively; (**b**) presents the lower-limb exoskeleton modules that capture the force/torque generated by the user implementing a sensory interface and a processing module, the actuation system and the mechanical structure generate the calculated torque and transmit the torque to the user's lower-limbs

example, the interface for acquiring EMG is placed on the user's muscle groups and for EEG acquisition. For this reason, the literature shows other alternatives where communication between the user and the wearable robot is generated. In this sense, the estimation of (pHRI) has been proposed [19–21]. In contrast to the cHRI, the pHRI evaluates some parameters that estimate the force/torques generated between the user and the wearable robot [22]. These parameters do not estimate the cognitive process in which the motion is generated as presented in the cHRI. The estimation of pHRI is usually implemented in lower-limb exoskeletons to assist or complement the user's movements in therapy sessions. This information is used as input to various control strategies to generate force/torque or angular velocity applied by the wearable robot employing a mechanical structure or actuation system.

The pHRI recently mentioned is applied in various workspaces. The literature has defined different categories of pHRI: the supportive category, where the robot device does not execute the task, this primary function is providing the tools to the user that develop the task [23]; collaborative category, the user and the robotic device develop the activity; and the cooperative category includes the interaction forces between the user and the robotic device, is to say, the robot and the user work in direct physical contact [21, 23]. In this sense, the lower-limb exoskeletons and the user are classified into a cooperative category. Using these interaction forces

and control strategies generates natural user primitive movements using lower-limb exoskeletons [24, 25].

Currently, multiple tools are implemented to estimate the user's movements, where some of these methods are equipped in the lower-limb mechanical structure. For example, Strain gauges are located in the robotic device mechanical structure to calculate the lower-limb movement perceived by the exoskeleton [12, 26]. As a result, each lower-limb exoskeleton joint is used as a force/torque sensor [27]. The force sensor implementation depends on the mechanical structure morphology of the device and the anatomical plane of the human body from which it is desired to estimate these forces. The use of force sensors in the mechanical structure simplifies the use of pHRI-based control strategies. Besides, no user instrumentation is required and system calibration is performed in a short period.

In conclusion, this section explains the generation of the pHRI between the user and the lower-limb exoskeleton that implements the user's movements (force/torque), which categorized the pHRI in the user and the wearable robot. Additionally, Fig. 8.1 describes the method where pRHI and the outcome calculated by the wearable robot. In this sense, the following section presents the methods applied in the lower-limb movements estimation and the force/torque acquisition, establishing the inputs in implementing some control strategies based on the pHRI.

8.3 Sensors in the HRI of the AGoRA Lower-Limb Exoskeleton

The pHRI has focused on bidirectional communication between the exoskeleton and the patient. This development requires various sensors located in the exoskeleton mechanical structure and the user's lower limbs. As an example, the use of force sensors, incremental and absolute encoders, and IMU sensors can allow the estimation of patient force, angular position of the joints, and the estimation of space-time parameters of some sections of the lower limbs for the recognition of various tasks. This section comprises the sensory interface configuration used in the *AGoRA* lower-limb exoskeleton in the estimation of these parameters. To learn the modules that involve a lower-limb exoskeleton, this section presents the information applied as an input for the acquisition of the lower-limbs movements and the force/torque estimation to apply the pHRI in the design of some control strategies.

8.3.1 Force Sensing

The interaction forces estimation between users and rehabilitation devices provides the implementation of stationary therapy [28], and the execution of several activities where an exoskeleton complements the user's movements [29]. Generally, resistive sensors have been used in robotic devices such as lower-limb prostheses [30] and lower-limb exoskeletons [12, 26, 30, 31] to acquire the forces generated by the user using the rehabilitation or assistance wearable robot. The *AGoRA* exoskeleton use

strain gauges (632–180, RS Pro, UK) located in the link of the robotic device. As a result, the strain gauge measures the link deflection caused by the user's lower-limb movements. In this way, the user movements generate deflections in different sections of the mechanical structure. Hence, the force/torque sensor is comprised of each link of the *AGoRA* exoskeleton instrumented by the Strain gauge. Consequently, the user's lower-limb force/torque is estimated in terms of (Nm) and implemented as an input of the pHRI control strategies. The force-torque sensor development is divided into sensor location and value acquisition, and signal processing and characterization.

The sensor location and value acquisition comprise the mechatronic integration for the force sensor reading and signal processing. Generally, the force sensor measurement is acquired using either a half Wheatstone bridge configuration or a full Wheatstone bridge configuration. These configurations do not affect the measured value of the force sensor by temperature fluctuations. Figure 8.2 shows an example of the strain gauge location based on the motion intention acquisition in the sagittal plane of the user's thigh and shank. Subsequently, an analog-to-digital conversion (ADC) and a signal amplification step are performed. Finally, the acquired signal is filtered applying a mean filter where the torques data is stored in a vector (mean_v(n)) and is calculated the average vector value. The next vector sample delete the value stored in the vector zero position (mean_v(0)), move each vector data to the left one position, store a new data in the vector n position (mean_v(n)), and recalculate the average value of this vector. As a result, the signal is smoothed.

The signal processing and characterization involve the characterization of the filtered signal, where the acquired value will be expressed in terms of torque (Nm). The filtering and characterization process requires embedded systems adapted for implementing digital filters and ensuring the real-time acquisition of these parameters. For example, the *AGoRA* exoskeleton uses devices such as a RasberryPi to apply the digital filters and implement the force sensor characterization function. The main objective of the sensor characterization process is to calculate the rate of change of the force generated in the sensor vs the voltage variation generated in the Wheatstone half-bridge. Generally, the behavior of these sensors shows a linear behavior expressed by the function $\tau = mx + b$ showed in Fig. 8.2. Where τ represents the force/torque value, m is the change ratio of the force/torque vs voltage value, and x is the value obtained by the force sensor. The value of b equals the value acquired by the force sensor at a force/torque of 0 [N]/ 0 $[Nm]$.

8.3.2 Position and Motion Sensing

Lower-limb exoskeletons implement various control strategies that use parameters such as angular position and angular velocity, which are acquired from the hip, knee, and ankle joints in the three anatomical planes of the human body [32, 33]. The acquisition of these parameters is aimed to monitor the effectiveness of the lower-limb exoskeleton. Additionally, the kinematic parameters acquisitions are

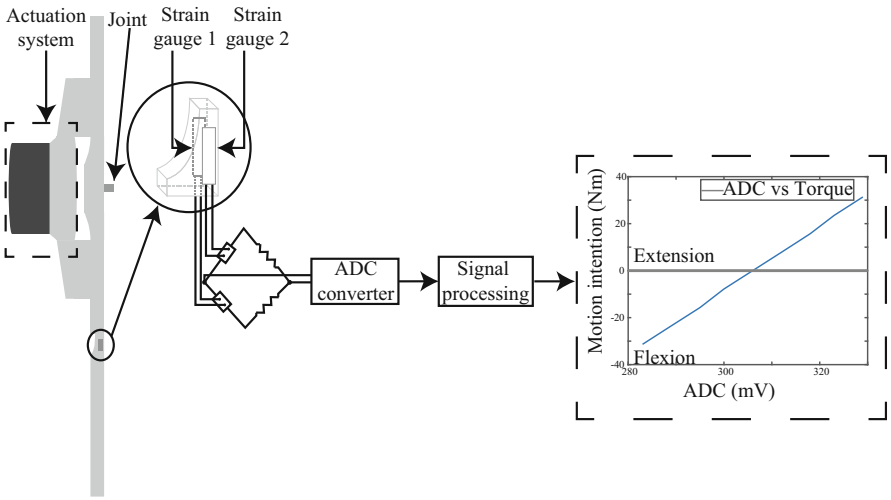

Fig. 8.2 Strain gauge's location and the data processing to obtain the user's generated torque and transmitted to the exoskeleton's mechanical structure

implemented as an input of the control strategies generating calculated torques or gait trajectories to rehabilitation and assistance.

The kinematic parameters acquisition is performed through encoders. These sensors allow estimating the angular position and the angular velocity of the exoskeleton joints. Two types of encoders are used for these applications. The first is the incremental encoder, which counts the motor shaft turns using the encoder position when powered. This feature may represent a disadvantage for exoskeletons adapted to develop more than one activity of daily living. This sensor is used in exoskeletons for stationary therapy [34–36] and the development of various actuation systems focused on the pHRI [37,38]. The second is the absolute encoder that provides a reference axis to the joints of lower-limb exoskeletons. Generally, the absolute encoder is used in lower-limb exoskeletons focused on assistance and rehabilitation. Figure 8.3 shows the magnetic encoder location for each joint of the *AGoRA* exoskeleton.

The implementation of this sensor in lower-limb exoskeletons can be done in several ways depending on the sensor composition offered by the provider. For example, the AGoRA exoskeleton uses absolute magnetic encoders (AS5600, ams AG, Austria). The sensor instrumentation requires performing sensor location on the lower-limb exoskeleton structure, filtering, and sensor characterization. For this case, the encoder location is performed directly on the center of rotation (CR) of each joint of the exoskeleton as seen from the sagittal plane. The ADC is performed by the magnetic encoder mentioned above. The behavior of the magnetic encoder is expressed by the function $\theta = mx + b$. Where m is equivalent to 0.01371 and indicates the change ratio of the angular position with the voltage value. The value of x is equivalent to the value obtained by the magnetic encoder. Finally, b equal to

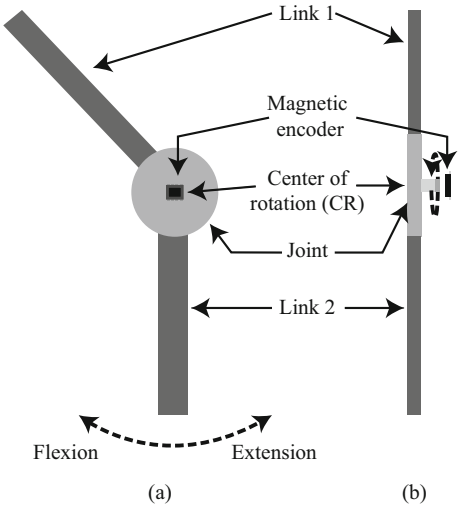

Fig. 8.3 Presents the magnetic encoder located in the Center of Rotation (CR) in the lower-limb exoskeleton joint. The figure shows the sensor location in the sagittal plane (**a**) and the frontal plane (**b**)

the magnetic encoder value where the joint angular position equal to 0° for the hip and knee joints.

IMU sensors provide data related to the angular position, angular velocity, and angular acceleration in various coordinate axes. These tools are applied to monitor patient movements, classify activities of daily living using machine learning methodology [39–41], or apply the acquired parameters as an input to various control systems. These applications allow increasing user's participation in therapy sessions [42]. In this way, it is possible to define an assistance level in various robotic assistive and rehabilitation devices [43]. For instance, A gait phase detection algorithm mentioned in Chap. 5 is implemented in the AGoRA exoskeleton Control strategies to support the user's gait pattern. This classifier uses an IMU sensor to acquire the inputs in control systems. For example, Chap. 5 presents an online gait phase detection module applied in the *AGoRA* exoskeleton.

8.4 Actuation in the HRI of the AGoRA Lower-Limb Exoskeleton

As mentioned in Sect. 8.3, obtaining the kinematic and kinetic parameters allowed defining the inputs for the various control strategies. Subsequently, this information is processed to estimate the system response. This response expressed in terms of torque, angular velocity, or angular position is generated as mechanical energy transmitted to the user's joints. For this purpose, the lower-limb exoskeletons are composed of a mechanical structure that provides the coupling between the wearable robot and the user. Additionally, an actuation system generates this mechanical energy to complement the user's movements in the execution of walking activity.

The *AGoRA* lower-limb exoskeleton consists of a rigid structure composed of 2 active joints on the right limb to assist flexion/extension movements for the hip and knee joints. Additionally, a passive joint enables abduction and adduction movements in the patient's hip [27]. The rigid structure is made up of duraluminium, lightweight, resistant, and low-corrosion material [27]. Additionally, the links coupled with the thigh and shank are telescopic bars, which are adjusted according to the user's anthropometric measurements. Thus, the device can be used by people between 1.70 and 1.83 m tall with an approximate weight of 90 kg.

The *AGoRA* lower-limb exoskeleton is equipped with stiff actuators to generate the required torques in the user's lower limbs. This actuation system comprises brushless DC electric motors (EC-60 flat 408057, *Maxon Motor AG*, Switzerland), which can provide a nominal torque of 0.228 Nm, reaching a maximum of 6000 rpm or 628.318 rad/s [44]. Taking as reference the torque values generated to assist using 50–80 Nm exoskeletons [45,46], the actuation system is complemented with a speed reduction gearbox (CSD-20-160-2AGR, *Harmonic Drive LLC*, USA) with a gear ratio of 160:1. As a result, torques of 35 Nm nominal and 180 Nm peak torque are generated, with an angular velocity of 37.5 rpm or 3.92 rad/s, torques and angular velocity similar to [47].

8.5 Impedance Control of Human–Robot Interaction

Literature shows the modeling of a lower-limb exoskeleton through the concepts of an n degree of freedom manipulator robot. Robot dynamics is generated, defined as a compensation system to forces/torques that affect the robot's movement. Subsequently, the wearable robots present several behavioral models of active actuation systems based on the mass-spring-damper system implementation and a mass-damper system. As a result, several control strategies are implemented that consider the forces/torques generated in the pHRI. In this sense, an impedance control applied in wearable robot proposed two concepts considering the generation of calculated force/torque or change the joint's stiffness according to the lower-limb exoskeleton workspaces. This section aims at defining these concepts from the viewpoint of the *AGoRA* lower-limb exoskeleton. This section will be covered as follows: (1) problem statement, where the *AGoRA* exoskeleton dynamics and the definition of a mass-spring-damper system will be explained, and two types of impedance control (2) impedance controllers; and (3) admittance controllers.

8.5.1 Problem Statement

Control strategies applied to lower-limb exoskeletons involve two key concepts. The first defines the forces/torques that are present in the wearable robot. As an example, moments of inertia, gravity, friction, among others are defined. The definition of these parameters is named the Feedforward or the robot's dynamic system. The second is the implementation of a feedback system to the robotic device. Therefore,

a mass-spring-damper system or a mass-damper system is used in the exoskeleton joints. In this sense, this section shows the key concepts for implementing the control system for a lower-limb exoskeleton.

8.5.1.1 Robot's Dynamics

The development of control strategies for a lower-limb exoskeleton involves the estimation of two relevant factors. One of these focuses on the forces/torques identification to generate the lower-limb exoskeleton joints motion. The second implements the pHRI and the lower-limb movements to estimate the motion generated by the actuation systems. Each of these factors is involved as system feedback and feedforward, respectively. In this sense, this section shows the feedforward estimation of a lower-limb exoskeleton. Note that exoskeletons present various kinematic models. In this section, the kinematic model for the AGoRA exoskeleton will be presented as an example.

The exoskeleton feedforward estimation is performed using applied concepts to manipulator robots. One of these involves the total energy calculation of the system by obtaining the kinetic energy and the potential energy related to the exoskeleton links. This is expressed in Eq. 8.1:

$$\varepsilon = \kappa(q, \dot{q}) + U(q). \tag{8.1}$$

The estimation of these energies involves the conservative and non-conservative forces of the system. Using the Lagrange equation of motion (Eq. 8.2), the compensation system value is obtained, expressed in torque (Nm).

$$[L] = \kappa(q, \dot{q}) - U(q, \dot{q}). \tag{8.2}$$

The differential kinematics value for each link must be estimated to obtain this value for a device such as the *AGoRA* exoskeleton. This will provide information on the angular velocity of the robot link at an instant of time. For this purpose, Eqs. 8.3 and 8.4 are used by applying the geometric Jacobian expressed in Eq. 8.5:

$$Link_{1(x,y)} = \begin{bmatrix} l_{c1} \sin q_1 \\ -l_{c1} \cos q_1 \end{bmatrix} \tag{8.3}$$

$$Link_{2(x,y)} = \begin{bmatrix} l_1 \sin q_1 & l_{c2} sen(q_1 + q_2) \\ -l_1 \cos q_1 & -l_{c2} \cos(q_1 + q_2) \end{bmatrix} \tag{8.4}$$

$$\begin{bmatrix} \Delta x \\ \Delta y \end{bmatrix} = \begin{bmatrix} \frac{\delta F_x(q)}{dq_1} & \frac{\delta F_x(q)}{dq_2} \\ \frac{\delta F_y(q)}{dq_1} & \frac{\delta F_y(q)}{dq_2} \end{bmatrix} \begin{pmatrix} \Delta q_1 \\ \delta q_2 \end{pmatrix}. \tag{8.5}$$

In this sense, the differential kinematic for the lower-limb joints is presented in Eqs. 8.6 and 8.7:

$$\upsilon_1 = \begin{bmatrix} l_{c1} \cos q_1 \\ -l_{c2} \sin 1_1 \end{bmatrix} \dot{q_1} \tag{8.6}$$

$$\upsilon_2 = \begin{bmatrix} l_1 \cos q_1 + l_{c2} \cos q_1 + q_2 & l_{c2} \cos q_1 + q_2 \\ l_1 \sin q_1 + l_{c2} \sin q_1 + q_2 & l_{c2} \sin q_1 + q_2 \end{bmatrix} \begin{bmatrix} \dot{q_1} \\ \dot{q_2} \end{bmatrix}, \tag{8.7}$$

where l_1 is the link 1 length, l_{c2} is the center of mass for the link 2 joint length, q_1 and q_2 are the joint's angular position. The next step to calculate the total system energy is the estimation of the exoskeleton kinetic energy. This parameter is expressed in Eq. 8.8:

$$\kappa = \sum_{i=1}^{n} \frac{1}{2} m_i {\upsilon_i}^T \upsilon_i + \frac{1}{2} I_i^2 {\dot{q}_i}^2. \tag{8.8}$$

Equation 8.8 presents the kinetic energy. In the lower-limb exoskeleton, where m_n is the link mass, υ_n is the differential kinematic, I_n the link inertia moment. Finally, $\dot{q_n}$ is the angular velocity for each joint. In this order, the kinematic energy of the *AGoRA* lower-limb exoskeleton is expressed in Eq. 8.9:

$$\begin{aligned} \kappa = & \frac{1}{2} \left[m_2 l_1^2 + I_1^2 + I_2^2 + m_2 l_1^2 + m_2 l_{c2} + 2 m_2 l_1 l_{c2} \cos q2 \right] \dot{q_1} \\ & + \frac{1}{2} \left[I_2 + m_2 l_{c2}^2 \right] {\dot{q_2}}^2 + \left[m_2 l_1 l_{c2} \cos q_2 + m_2 l_{c2} + I_2 \right] \dot{q_1} \dot{q_2}. \end{aligned} \tag{8.9}$$

The second step in calculating the Lagrange equation of motion is estimating the potential energy that involves the conservative forces. This parameter is expressed in Eq. 8.10:

$$U(q) = mgh, \tag{8.10}$$

where m is the link mass, g is the gravity acceleration value. This function is applied for each *AGoRA* exoskeleton link. The *AGoRA* exoskeleton potential energy is expressed in Eq. 8.11:

$$U(q) = mgl_{c1}[1 - \cos q_1] - m_2 g[(l_1)]. \tag{8.11}$$

8.5.1.2 The Mass-Spring-Damper System

The mass-spring-damper system is the concept applied in the joints of robotic devices, whose main function is focused on applying pHRI [48]. The implementation of this system in the knee and hip joints approximates the human muscle biomechanical model. Currently, the literature presents the human muscle as a component composed of a spring-like elastic element in parallel with a viscous element [48–50]. Implementing this concept in the knee and hip actuators assists the actuated limb through calculated torques [50]. Additionally, the patient participates in developing the motion to complement the movements generated by the lower-limb exoskeleton [50]. This section comprises the definition of the mass-spring-damper system applied in various mid-level control strategies for lower-limb exoskeletons. Some examples of the implementation of this concept for the *AGoRA* exoskeleton will be shown.

The mass-spring-damper system is mainly composed of a spring element and a damping element. The spring element is referred to as a force restoring component. The response of this element is expressed in terms of force, where the elongation of the element is multiplied with the spring elasticity constant [51, 52]. On the other hand, a delaying element is required to decrease the system oscillations generated by the spring element. For this purpose, a damping element is implemented to provide stiffness to the system. The system's response is expressed in terms of force, which depends on the linear velocity of the system, multiplied with a viscosity constant characteristic of a damper [51,52], resulting in a retarding force to the force generated by the spring element.

The implementation of this system has been called an impedance controller proposed in 1984 [48]. This controller presented an interaction method between a manipulator robot and the workspace environment using calculated forces. Subsequently, it was implemented to apply the pHRI concept to lower-limb exoskeletons for various purposes [36, 53]. Lower-limb exoskeletons such as the AGoRA exoskeleton implement this system at the hip and knee joints for sagittal plane assistance as seen in Fig. 8.4. Although this exoskeleton does not have an actuation mechanism based on a physical mass-spring-damper system at each joint, it applies the system virtually using the Eq. 8.12:

$$F = -\overbrace{k(x_d - x)}^{spring} - \overbrace{\beta(\dot{x_d} - \dot{x})}^{damping}, \tag{8.12}$$

where k equals the elasticity constant, x_d represents the desired position, and x is the joint's actual position, the operation of these constants represents the elastic element's effect on the joint. Additionally, β is the viscosity constant of the system, $\dot{x_d}$ equals the desired velocity of the system, and $\dot{x}$ equals the system's actual velocity. These parameters and the operation of these constants represent the effect of the damping element on the joint. For a mass-spring-damper system to be in equilibrium, the sum of these forces would equal zero (0), so Eq. 8.12 is expressed in Eq. 8.13:

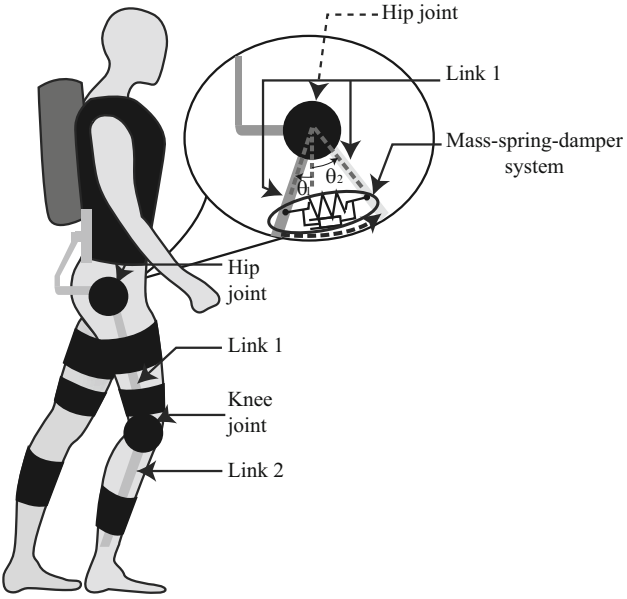

Fig. 8.4 Lower-limb exoskeleton schematic implementing the mass-spring-damper system in the knee and hip joints

$$\begin{aligned} 0 &= m\ddot{x} + \beta(\dot{x_d} - \dot{x}) + k(x_d - x) \\ &= \ddot{x} + \frac{\beta}{m}(\dot{x_d} - \dot{x}) + \frac{k}{m}(x_d - x). \end{aligned} \tag{8.13}$$

If $\frac{\beta}{m}$ equal to 2λ and $\frac{k}{m}$ is ω^2, Eq. 8.13 represents

$$\ddot{x} + 2\lambda(\dot{x_d} - \dot{x}) + \omega^2(x_d - x) = 0 \tag{8.14}$$

$$r^2 + 2\lambda r + \omega^2 = 0. \tag{8.15}$$

As a result, Eq. 8.15 is equal to a second-order system where $\ddot{x}$ is the acceleration, $\dot{x}$ velocity, and x equal to the system's position. This equation provides the k and β system values.

The application of this concept and its a variation in the various actuation systems comprise the mid-level control strategies. These are based on the acquisition or generation of torque profiles that complement the lower-limb movements of a stroke patient. As has been shown, the lower-limb movements are a significant factor that will allow the patient to be included in the control strategy of the device. The

following sections will present two control methods based on this concept to develop mid-level control strategies.

8.5.2 Impedance Controller

The impedance controller presented by Hogan et al. in [48] has been fundamental in the development of control strategies applying the lower-limb movements for rehabilitation devices. Its performance mainly focuses on varying the assistance level provided by the device, by increasing or decreasing the maximum torque profile transmitted by the actuation system [53–55]. The development of the impedance controller is implemented employing a mass-spring-damper system as shown in Fig. 8.5a.

This system considers inputs to the system kinematic parameters such as the angular position and angular velocity of the lower-limb exoskeleton joints to obtain a calculated torque profile applied to the actuation systems (Fig. 8.5b). In this sense, the impedance controller is considered a restoring element of forces that varies according to the value of the spring element elasticity constant(k) shown in Eq. 8.16:

$$\tau = \overbrace{k(q_d - q)}^{spring} + \overbrace{\beta(\dot{q_d} - \dot{q})}^{damper}. \tag{8.16}$$

The k and β are the elasticity constant and the damping constant, respectively, q_d equal to the desired joint angular position; q is the current joint position, $\dot{q_d}$ equal to the desired angular velocity. In this case, when the joint angular position is equal to

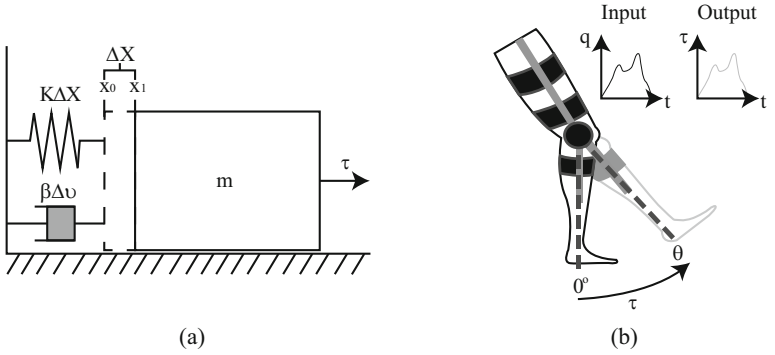

Fig. 8.5 Impedance controller presentation; (**a**) impedance controller schematic using a mass-damper system where the $\beta \times \triangle v$ equal to the damper element torque response, $K \times \triangle X$ equal to the spring element torque response, and τ is the impedance controller output; (**b**) shows the impedance controller applied in the lower-limb exoskeleton's joint, where the input signal is the joint angular position, the impedance controller response is a calculated torque applied in the joint

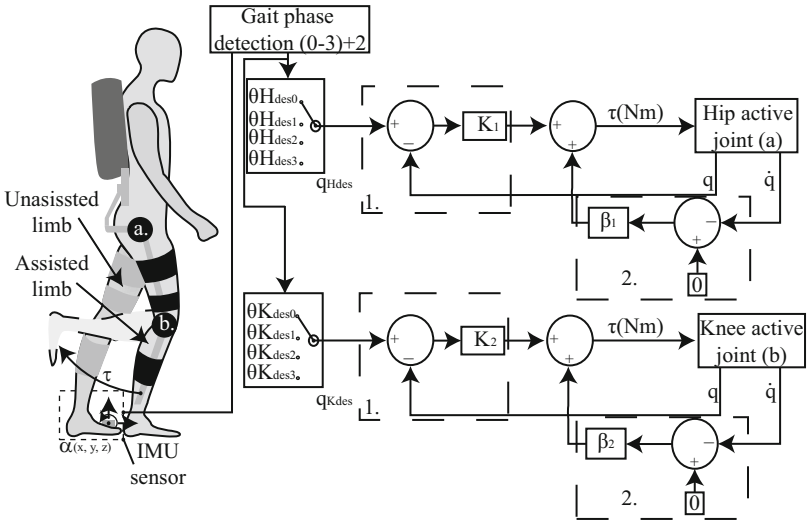

Fig. 8.6 Assistance mode schematic; the IMU sensor is located in the foot tip to the non-assisted limb to estimate the angular acceleration ($\alpha_{(x,y,z)}$); this parameter is applied input signal of the gait phase detection module. As a result, the gait phase detection module provides a number in the range from zero to three according to the phase gait detected. The unassisted limb gait phase equals to the assisted limb gait phase ahead of two phases. This detected phase as an input for a desired angular position selector for the hip ($\theta H_{des}0$, $\theta H_{des}1$, $\theta H_{des}2$ and $\theta H_{des}3$) and the knee ($\theta K_{des}0$, $\theta K_{des}1$, $\theta k_{des}2$ and $\theta k_{des}3$) joints. This value is operated for the mass-spring(1.)-damper(2.) system to calculate the actuation system's torque

the joint desired angular position, the desired angular velocity equal to zero. Finally, $\dot{q}$ represents the joint current angular velocity.

The assistance mode of the *AGoRA* exoskeleton, showed in Fig. 8.6, implements an impedance controller for the hip and knee joints that requires the estimation of the parameters of the spring element and the damping element. This control strategy guides each joint to the desired position, providing corrections employing torque profiles. In this way, the patient is involved in the task, making movements in the same direction in which the device applies the assisting torque. Once the gait phase is identified (by employing the sensors IMU [43]), the desired angular position values are established for each gait phase used as input to the impedance controller.

The assistance mode is developed for people with right-sided hemiparesis, where the robotic device considers the movements of the unaffected limb. Therefore, the left limb is instrumented with a 9 degree of freedom IMU sensor for the user's gait sub-phase detection used as input to the control strategy. The values of this input parameter are given in a value from 0 to 3, where Heel Strike equals zero, Flat Foot equals 1, Heel Off equals 2, and the Toe Off phase equals 3. Each sub-phases a desired angular position is assigned to the joint assisted by the *AGoRA* exoskeleton. Taking into account what was presented in Villa Parra et al. [26], El Zahraa Wehbi

et al. [34], and Webster et al. [56], the gait characteristic as a symmetric activity, it is identified that the gait phase that the assisted limb should execute corresponds to 2 sub-phases in advance of the four detected gait sub-phases of the unaffected limb.

It is necessary to keep into account that this control is designed to provide an assistance level. Therefore, the adjustment of these variables depends directly on the assistance level required in the walking activity. An approximation of the estimated values for these variables is made using an approximation of the Eq. 8.15 in Eq. 8.17:

$$\ddot{q} + 2\lambda\Delta\dot{q} + \omega^2\Delta\dot{q} = 0 \tag{8.17}$$

$$2\lambda = \frac{\beta}{ml^2} \tag{8.18}$$

$$f_n = \frac{\omega_n}{2\pi} \tag{8.19}$$

$$\omega_n = \sqrt{\frac{k}{ml^2}}. \tag{8.20}$$

To apply Eq. 8.17, λ is defined in Eq. 8.18, where β is the damping constant, m is the lower-limb mass that involves the thigh mass and the shank mass, l is the thigh and shank length. In Eq. 8.19 the bandwidth is defined as equals to $f_n = 0.5936$ Hz. Finally, in Eq. 8.20 k is the elasticity constant. These equations are taken into account to estimate the k and β varying the assistance level and the system stiffness [57].

8.5.3 Admittance Controller

Admittance control is focused on acquiring human–robot interaction forces in the implementation of haptic applications [58,59]. This characteristic allows to simulate the stiffness of a system virtually, or the system inertia to be reduced employing this strategy [22]. This same principle is applied to robotics for rehabilitation and assistance of people with some neurological disease. Exoskeletons such as *ALLOR* (Federal University of Espirito Santo, Brazil) developed for walking, feature an admittance controller that changes the system stiffness at different gait phases [26]. *BioMot* (Future and Emerging Technologies (FET), Spain) applies this control to decrease the inertia of the exoskeleton to provide movement freedom for the identification of the user's gait pattern [60]. Likewise, the knee orthoses used in stationary therapy use an admittance controller to record the therapy trajectory to be performed, complemented by an impedance controller executed in the trajectory reproduction. The implementation of an admittance control in rehabilitation and assistance robotics becomes a significant contribution. It allows the patient to be

involved in the control strategy applied to the device, without requiring the patient's instrumentation using invasive sensors.

The literature shows that the implementation of this kind of control using a mass-spring-damper system in each joint of the exoskeleton or robotic orthosis [16]. However, implementing a spring element may affect the system response because the force generated by a person does not necessarily correspond to a desired angular position. Therefore, in some cases an admittance control is not developed for the generation of restoring forces. For this reason, some lower-limb exoskeletons implemented a mass-damper system for the hip and knee joints [26]. This system provides for a viscous coefficient that varies the inertia of the exoskeleton joints, obtaining different levels of stiffness in the system. In rehabilitation and assistance of lower limbs, applied methodologies are focused on providing assistance when needed (AAN) [61]. This concept uses this type of control by taking advantage of the force generated by the patient and used for therapy sessions in gait rehabilitation. As a result, an admittance control allows a device to be called back drivable.

Currently, several ways of implementing this theory can be identified which depend on the actuation system used in the lower-limb exoskeleton. Some actuation systems use a physical mass-damper system by using a damping element in the joint. Other devices use a rigid actuator which generates an angular velocity response at the joint. These actuation systems complement a sensory interface that will enable the device the force/torque user's estimation.

The control strategy based on an *AGoRA* exoskeleton admittance control considers a rigid actuation system. This system is coupled to the mechanical structure of the exoskeleton which is instrumented with force sensors mentioned in Sect. 8.3.1, for the estimation of the force/torque estimation. In this sense, admittance control in the *AGoRA* exoskeleton is implemented, where the system input is the pHRI expressed in terms of torque, and the response to the system is implemented by the actuation system in terms of angular velocity, as shown in Fig. 8.7b. As a result, the device generates movements on the joints according to the patient's voluntary movements. The *AGoRA* exoskeleton follows the patient's movements simulating a back drivable device, or it can operate as a rigid device according to the value of the damping constant configured for the system.

The admittance controller is defined in Eq. 8.21:

$$\tau = \beta(\dot{q_d} - \dot{q_c}), \tag{8.21}$$

where τ equals the torque to be generated by the damping element, $\dot{q_d}$ is the desired velocity, and $\dot{q_c}$ is equal to the current angular velocity of the joint, the admittance controller applied in the *AGoRA* exoskeleton is showed in Fig. 8.7.

The transparency mode presented in Fig. 8.8 is implemented using the admittance controller on the hip and knee joints. This control strategy can change the inertia of each lower-limb joint, produced by the implementation of gearboxes coupled with the exoskeleton actuators.

As is showed in Fig. 8.8, the transparency mode comprises the torque acquisition. Hence, the thigh torque is estimated using the calculated torque sensed by the Strain

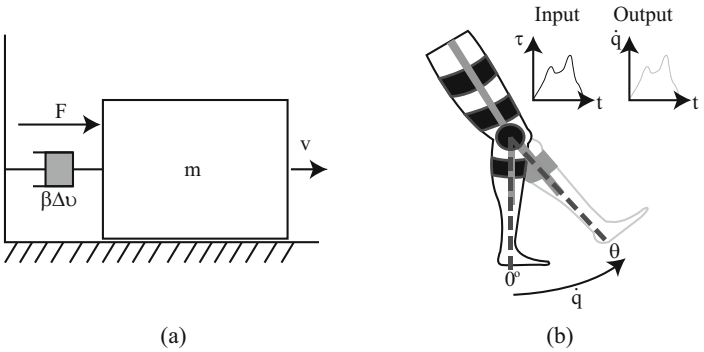

Fig. 8.7 Admittance controller presentation; (**a**) admittance controller schematic using a mass-damper system where the $\beta \times \Delta v$ equal to the damper element torque response, F is the applied force in the system, and v is the admittance controller outcome; (**b**) shows the admittance controller applied in the lower-limb exoskeleton's joint, where the input signal is the torque generated transmitted to the lower-limb mechanical structure, the admittance controller response is an angular velocity applied in the joint

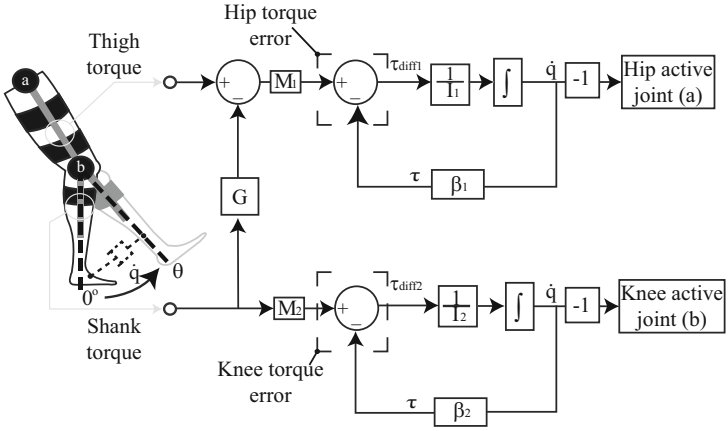

Fig. 8.8 Transparency mode schematic; the thigh and shank torque are estimated in terms of torque. The thigh torque value, and the shank torque value are operated with M_1 M_2 to attenuate the torque value. Subsequently, these parameters are applied into ad admittance controller to generate angular velocity in each actuation system's joint

gauge located in the thigh. Subsequently, this value is operated with the shank torque multiplied by a G gain. As a result, the real thigh torque value generated by the user's hip is calculated. The thigh and shank torque generated by the hip and the knee user's joint, are used to estimate the hip and knee torque error to obtain the difference between the joint torque and the torque obtained from the damper element. The next step in the estimation of the admittance controller response uses the torque error (τ_{diff}) divided into inertia moment (I) for each joint ($I = l \times m$)

where m equal to the joint's mass and l equal to the length for each link. This value is operated using an integral by obtaining the joint's angular velocity ($\dot{q}$). Finally, the rotational orientation of the joint generated by the gearbox is corrected by multiplying the angular velocity value by a factor of -1. As a result, the system produces angular velocity profiles applied to the actuation system according to a user's lower-limb movements estimated by the force sensors.

The transparency mode is organized as follows:

- **Torque acquisition:** Corresponds to the torque acquisition for the thigh and shank sections.
- **Calculate the angular velocity:** Estimating the τ_{diff} through the torque for each joint and the torque generated by the damper element. Subsequently, the division of the inertia moment and the integral of the obtained value.
- **Generate the torques through the actuation system:** The angular velocities are sent for each actuation system to generate movements in the hip and the knee user's joints.

8.6 Case Study: Impedance Control in the AGoRA Lower-Limb Exoskeleton

The test using the assistance mode was performed with a subject who does not suffer any gait pathology. The subject was a male, 1.72 m in height and weighed 73 Kg . The test environment is a flat surface of 20 m walked by the user in a flat surface in a straight line using the *AGoRA* exoskeleton. This device assisted the right limb in the hip and knee joints in the sagittal plane. In this case, the mode uses the joint angular position to correct the trajectory using calculated torque profiles. Figure 8.9 shows the response of the assistance mode in terms of angular position, and torque generated by the controller. Additionally, the system performance uses the gait phase detection module mentioned in Chap. 5 to assign a desired angular position for the hip and knee joints.

The gait assistance mode outcomes are showed at the hip and knee joint during three gait cycles. Figure 8.9a shows the angular knee position vs. the joint desired angular position. The knee joint showed different maximum knee flexion values in three gait cycles, considering the gait phases exhibited different periods. However, the desired angular position was adjusted according to the gait phase detection during the gait phase. As a result, the assistance mode output (Fig. 8.9b) generated several peak torques that were adjusted according to the desired angular position. Additionally, the implementation of impedance control in assistance mode fulfills the objective of generating calculated torques that complement the user's movement. Which is to say, there is not a 100% assistance level assistance. For this reason, an error between the desired angular position and the angular knee position is observed in the test. The system can be adjusted to provide a higher assistance level than the test by increasing the value of the system's elasticity constant (k). As a result, this would decrease the error shown in Fig. 8.9.

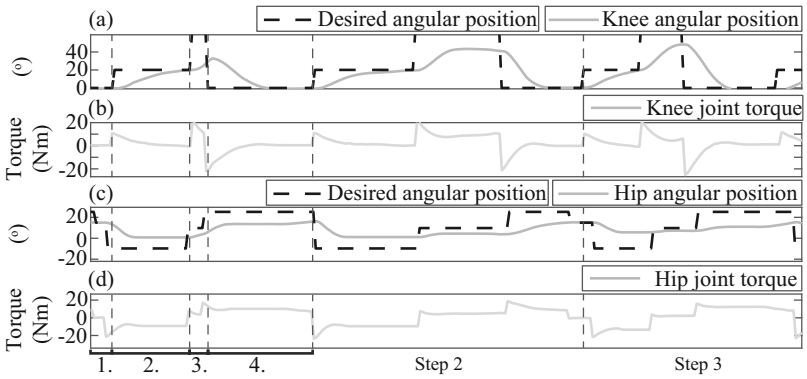

Fig. 8.9 Assistance mode outcome implemented for the walking activity in a healthy user; (**a**) shows the angular knee position in comparison to the desired angular position; (**b**) shows the assistance mode response for the knee joint in terms of torque (Nm); (**c**) presents the hip angular position in comparison to the desired angular position; (**d**) shows the assistance mode response for the hip joint in terms of torque (Nm); 1.-"*Heel Strike*," 2.-"*Flat Foot*," 3.-"*Heel Off*," 4.-"*Toe Off*"

In the hip joint actuation, similar behavior is observed in Fig. 8.9.c shows an error between the angular position of the hip and the angular position as the system complements the motion performed by the user. The desired angular positions at the hip are adjusted according to the gait phase detection module. As a result, the system response generated peak torques to guide the joint to the desired position. Each calculated torque profile is adjusted according to the system's desired position; increasing the elasticity constant of the controller will decrease the angular position error presented at the hip.

8.7 Case Study: Admittance Control in the AGoRA Lower-Limb Exoskeleton

The test performed using the transparency mode was executed with a subject who does not suffer any gait-associated pathology. The subject is a male that is 1.72 m high and weighs 73 Kg. The test was developed on a flat floor surface of 7 m in length without obstacles. The subject wears the *AGoRA* lower-limb exoskeleton that actuates the right lower limb at the hip and knee joints in the sagittal plane during the test. As mentioned in Sect. 8.4, the stiff actuator joints of the *AGoRA* exoskeleton can simulate the back drivable response using an admittance controller applied in this transparency mode. Therefore, this test presented the controller response by showing the system input (thigh/shank estimation torque), the controller output expressed in angular velocity, and the knee joint response in terms of angular position. Figure 8.10 is presented the transparency mode outcome in the knee joint during the walking activity.

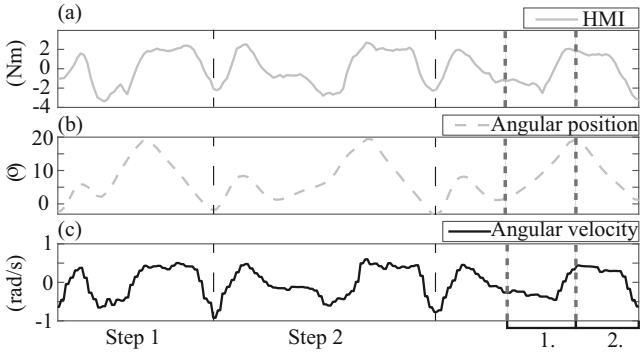

Fig. 8.10 Transparency mode response in the knee joint developing the walking activity. The response is shown in three knee gait cycles. Section 8.1. represents the knee flexion, Sect. 8.2. represents the knee extension; (**a**) presents the knee torque (Nm); (**b**) is the angular knee position during the walking activity; (**c**) equals to the transparency mode output in terms of angular velocity (rad/s)

The results of the pilot test in the walking activity are expressed in 3 gait cycles. The maximum torque generated was 4 Nm in knee extension and 2 Nm in joint flexion. As seen in Fig. 8.10a, the signal trajectory is not uniform to the angular knee position signal. However, the signal response is expressed into angular velocity profiles to obtain a smoothed response in the angular knee position. Likewise, the controller output signal is given since the admittance controller does not consider the joint's angular position. However, the signal is translated into angular velocity profiles and thus a smoothed trajectory of the angular knee position is obtained. Likewise, the behavior of the output signal of the admittance controller does not take into account the angular position of the joint. Finally, the ranges of motion observed in the knee joint are reduced compared to the ranges presented by a healthy person in a walking activity. The gain β is configured for the knee admittance controller that generates a stiffness in the joint that does not allow the free movement of the joint. On the other hand, the system stiffness is minor than generating joint motion with the rigid actuation system. The knee joint movements can be improved by increasing the value of the damper constant β of the admittance control.

8.8 Chapter Conclusions

This chapter presents the design of control strategies for a lower-limb exoskeleton. In this process, several tools that contribute to the development of these control systems were explained. The tools and concepts used in developing the *AGoRA* lower-limb exoskeleton are mentioned as an example. First, the pHRI was defined divided into different phases: (1) the generation of lower-limb movements by performing a process of acquisition, planning, and the user's lower-limb movement generation; (2) the pHRI estimation by the wearable robot, which processes

the information and provides a response as mechanical energy, generating the user's joint movements. Second, various inputs used in the pHRI estimation were presented, which mentioned the acquisition of kinetic and kinematic parameters and the signal characterization phase. In this process, the user's lower-limb movement acquisition options were non-invasive implementing a wearable robot in the walking activity. Third, the function of the actuation system that generates the mechanical energy for the movement of each joint is defined. As a complement, the mechanical structure that composes the *AGoRA* exoskeleton is mentioned in the aspects of the material that composes it and DoF, where it fulfills the primary function of being the coupling between the wearable robot and the user's joints.

In the analysis of the processing phase, the critical concepts for implementing the control strategies of the *AGoRA* exoskeleton are mentioned. In this way, the design of the robot dynamics and critical concepts of implementing a mass-spring-damper system and a mass-damper system were presented. As a result, the applied control concepts for the use of force/torque within the control strategies are introduced. As a result, the implementation of two control strategies, involving the integration of each module mentioned, is presented. As an example, the control strategies outcome was shown in a pilot study during the walking activity.

References

1. M.E. Mlinac, M.C. Feng, Assessment of activities of daily living, self-care, and independence. Arch. Clin. Neuropsychol. **31**(6), 506–516 (2016)
2. E. Peter, B. Deb, S. Sukesh, L. Shoshana, Activities of daily living (ADLs) (2021). https://www.ncbi.nlm.nih.gov/books/NBK470404/
3. A. Balaguer, Actividades de la vida diaria (2016)
4. C. Blomgren, K. Jood, C. Jern, L. Holmegaard, P. Redfors, C. Blomstrand, L. Claesson, Long-term performance of instrumental activities of daily living (IADL) in young and middle-aged stroke survivors: results from SAHLSIS outcome. Scand. J. Occup. Ther. **25**(2), 119–126 (2018)
5. K. Han, J. Lee, W.K. Song, Application scenarios for assistive robots based on in-depth focus group interviews and clinical expert meetings, in *2013 44th International Symposium on Robotics, ISR 2013* (2013)
6. J.-M. Belda-Lois, S.M.-d. Horno, I. Bermejo-bosch, J.C. Moreno, J.L. Pons, D. Farina, M. Iosa, M. Molinari, F. Tamburella, A. Ramos, A. Caria, T. Solis-escalante, C. Brunner, M. Rea, Rehabilitation of gait after stroke: a top down approach. J. NeuroEng. Rehabil. **66**, 66 (2011)
7. B. Koopman, E.H.F.V. Asseldonk, H.V.D. Kooij, Selective control of gait subtasks in robotic gait training: foot clearance support in stroke survivors with a powered exoskeleton. J. NeuroEng. Rehabil. **10**, 1–21 (2013)
8. L.D. da Silva, T.F. Pereira, V.R. Leithardt, L.O. Seman, C.A. Zeferino, Hybrid impedance-admittance control for upper limb exoskeleton using electromyography. Appl. Sci. **10**(20), 1–19 (2020)
9. S.C. Ouriques Martins, C. Sacks, W. Hacke, M. Brainin, F. de Assis Figueiredo, O. Marques Pontes-Neto, P.M. Lavados Germain, M.F. Marinho, A. Hoppe Wiegering, D. Vaca McGhie, S. Cruz-Flores, S.F. Ameriso, W.M. Camargo Villareal, J.C. Durán, J.E. Fogolin Passos, R. Gomes Nogueira, J.J. Freitas de Carvalho, G. Sampaio Silva, C.H. Cabral Moro, J. Oliveira-Filho, R. Gagliardi, E.D. Gomes de Sousa, F. Fagundes Soares, K. de Pinho Campos, P.F. Piza Teixeira, I.P. Gonçalves, I.R. Santos Carquin, M. Muñoz Collazos, G.E. Pérez Romero, J.I.

Maldonado Figueredo, M.A. Barboza, M. Celis López, F. Góngora-Rivera, C. Cantú-Brito, N. Novarro-Escudero, M. Velázquez Blanco, C.A. Arbo Oze de Morvil, A.B. Olmedo Bareiro, G. Meza Rojas, A. Flores, J.A. Hancco-Saavedra, V. Pérez Jimenez, C. Abanto Argomedo, L. Rodriguez Kadota, R. Crosa, D.L. Mora Cuervo, A.C. de Souza, L.A. Carbonera, T.F. Álvarez Guzmán, N. Maldonado, N.L. Cabral, C. Anderson, P. Lindsay, A. Hennis, V.L. Feigin, Priorities to reduce the burden of stroke in Latin American countries. Lancet Neurol. **18**(7), 674–683 (2019)
10. G.D. Whitiana, V. Vitriana, A. Cahyani, Level of activity daily living in post stroke patients. Althea Med. J. **4**(2), 261–266 (2017)
11. G. Colombo, M. Joerg, R. Schreier, V. Dietz, Treadmill training of paraplegic patients using a robotic orthosis. J. Rehabil. Res. Develop. **37**(6), 693–700 (2000)
12. J.L. Pons, Human-robot cognitive interaction, in *Wearable Robots: Biomechatronic Exoskeletons*, chap. 4 (Wiley, Hoboken, 2008)
13. A. Kilicarslan, S. Prasad, R.G. Grossman, J.L. Contreras-Vidal, High accuracy decoding of user intentions using EEG to control a lower-body exoskeleton, in *Proceedings of the Annual International Conference of the IEEE Engineering in Medicine and Biology Society, EMBS* (2013), pp. 5606–5609
14. A. Costa, R. Salazar-Varas, E. Ianez, A. Ubeda, E. Hortal, J.M. Azorin, Studying cognitive attention mechanisms during walking from EEG signals, in *Proceedings - 2015 IEEE International Conference on Systems, Man, and Cybernetics, SMC 2015* (2016), pp. 882–886
15. L.I. Minchala, F. Astudillo-Salinas, K. Palacio-Baus, A. Vazquez-Rodas, Mechatronic design of a lower limb exoskeleton, in *Design, Control and Applications of Mechatronic Systems in Engineering* (2017)
16. F.L. Haufe, A.M. Kober, K. Schmidt, A. Sancho-puchades, J.E. Duarte, P. Wolf, R. Riener, User-driven walking assistance: first experimental results using the MyoSuit *, in *2019 IEEE 16th International Conference on Rehabilitation Robotics (ICORR)* (2019), pp. 944–949
17. H. Kawamoto, S. Lee, S. Kanbe, Y. Sankai, Power assist method for HAL-3 using EMG-based feedback controller, in *Proceedings of the IEEE International Conference on Systems, Man and Cybernetics*, vol. 2 (2003), pp. 1648–1653
18. C. Castellini, P. Van Der Smagt, Surface EMG in advanced hand prosthetics. Biol. Cybern. **100**(1), 35–47 (2009)
19. S.K. Das, Adaptive physical human-robot interaction (PHRI) with a robotic nursing assistant. Ph.D. Thesis, University of Louisville (2019)
20. P.D. Labrecque, C. Gosselin, Variable admittance for pHRI: from intuitive unilateral interaction to optimal bilateral force amplification. Robot. Comput.-Integr. Manuf. **52**, 1–8 (2018)
21. A. Bicchi, M.A. Peshkin, J.E. Colgate, Safety for physical human–robot interaction. *Springer Handbook of Robotics* (Springer, Berlin, 2008) pp. 1335–1348
22. A.Q. Keemink, H. van der Kooij, A.H. Stienen, Admittance control for physical human–robot interaction. Int. J. Robot. Res. **37**(11), 1421–1444 (2018)
23. S. Haddadin, E. Croft, Physical human-robot interaction, in *Springer Handbook of Robotics* (Springer, Cham, 2016), pp. 1835–1874
24. I. Díaz, J.J. Gil, E. Sánchez, Lower-limb robotic rehabilitation: literature review and challenges. J. Robot. **2011**(i), 1–11 (2011)
25. A. Martínez, B.E. Lawson, M. Goldfarb, Preliminary assessment of a lower-limb exoskeleton controller for stroke rehabilitation in overground walking, in *IEEE International Conference on Rehabilitation Robotics* (2017)
26. A.C. Villa-Parra, D. Delisle-Rodriguez, J.S. Lima, A. Frizera-Neto, T. Bastos, Knee impedance modulation to control an active orthosis using insole sensors. Sensors **17**(12), 2751 (2017)
27. M. Sanchez-Manchola, D. Gomez-Vargas, D. Casas-Bocanegra, M. Munera, C.A. Cifuentes, Development of a Robotic lower-limb exoskeleton for gait rehabilitation: AGoRA exoskeleton, in *2018 IEEE ANDESCON Conference Proceedings* (2018), pp. 1–6
28. M.D. Sánchez Manchola, L.J. Arciniegas Mayag, M. Múnera, C.A. Garcia, Impedance-based backdrivability recovery of a lower-limb exoskeleton for knee rehabilitation, in *4th IEEE Colombian Conference on Automatic Control: Automatic Control as Key Support of Industrial Productivity, CCAC 2019 - Proceedings, (Medellin, Colombia)* (2019), pp. 1–6

29. T. Poliero, C. Di Natali, M. Sposito, J. Ortiz, E. Graf, C. Pauli, E. Bottenberg, A. De Eyto, D.G. Caldwell, Soft wearable device for lower limb assistance: assessment of an optimized energy efficient actuation prototype, in *2018 IEEE International Conference on Soft Robotics, RoboSoft 2018* (2018), pp. 559–564
30. J. Schuy, A. Burkl, P. Beckerle, S. Rinderknecht, A new device to measure load and motion in lower limb prosthesis - tested on different prosthetic feet, in *2014 IEEE International Conference on Robotics and Biomimetics, IEEE ROBIO 2014* (2014), pp. 187–192
31. M. Molinari, M. Masciullo, F. Tamburella, N.L. Tagliamonte, I. Pisotta, J.L. Pons, Exoskeletons for over-ground gait training in spinal cord injury. Biosyst. Biorobot. **19**, 253–265 (2018)
32. T. Bacek, M. Moltedo, K. Langlois, G.A. Prieto, M.C. Sanchez-Villamañan, J. Gonzalez-Vargas, B. Vanderborght, D. Lefeber, J.C. Moreno, BioMot exoskeleton - towards a smart wearable robot for symbiotic human-robot interaction, in *IEEE International Conference on Rehabilitation Robotics* (2017), pp. 1666–1671
33. A.J. Young, D.P. Ferris, State of the art and future directions for lower limb robotic exoskeletons. IEEE Trans. Neural Syst. Rehabil. Eng. **25**(2), 171–182 (2017)
34. F. El Zahraa Wehbi, W. Huo, Y. Amirat, M.E. Rafei, M. Khalil, S. Mohammed, Active impedance control of a knee-joint orthosis during swing phase, in *IEEE International Conference on Rehabilitation Robotics* (2017), pp. 435–440
35. W.M. Dos Santos, A.A.G. Siqueira, Impedance control of a rotary series elastic actuator for knee rehabilitation, in *The International Federation of Automatic Control (IFAC)*, vol. 19 (2014), pp. 4801–4806
36. A. Taherifar, G. Vossoughi, A.S. Ghafari, Variable admittance control of the exoskeleton for gait rehabilitation based on a novel strength metric. Robotica **36**, 427–447 (2018)
37. V. Grosu, C. Rodriguez-Guerrero, S. Grosu, B. Vanderborght, D. Lefeber, Design of smart modular variable stiffness actuators for robotic-assistive devices. IEEE/ASME Trans. Mechatron. **22**(4), 1777–1785 (2017)
38. L.M. Mooney, H.M. Herr, Biomechanical walking mechanisms underlying the metabolic reduction caused by an autonomous exoskeleton. J. NeuroEng. Rehabil. **13**(1), 1–12 (2016)
39. N. Abhayasinghe, I. Murray, Human activity recognition using thigh angle derived from single thigh mounted IMU data, in *2014 International Conference on Indoor Positioning and Indoor Navigation (IPIN 2014)* (2014), pp. 111–115
40. D. Micucci, M. Mobilio, P. Napoletano, UniMiB SHAR: a dataset for human activity recognition using acceleration data from smartphones. Appl. Sci. **7**(10), 1101 (2017)
41. B. Barshan, M.C. Yüksek, Recognizing daily and sports activities in two open source machine learning environments using body-worn sensor units. Comput. J. **57**(11), 1649–1667 (2013)
42. M.N. Victorino, X. Jiang, C. Menon, *Wearable Technologies and Force Myography for Healthcare* (Elsevier, Amsterdam, 2018)
43. M.D. Manchola, M.J. Bernal, M. Munera, C.A. Cifuentes, Gait phase detection for lower-limb exoskeletons using foot motion data from a single inertial measurement unit in hemiparetic individuals. Sensors **19**(13), 2988 (2019)
44. M. Motor, Maxon flat EC motor. Maxon (2017). https://www.maxongroup.com/medias/sys_master/root/8831018893342/2018EN-270.pdf
45. J.F. Veneman, R. Kruidhof, E.E.G. Hekman, R. Ekkelenkamp, E.H.F.V. Asseldonk, H. van der Kooij, Design and evaluation of the LOPES exoskeleton robot for interactive gait rehabilitation. IEEE Trans. Neural Syst. Rehabil. Eng. **15**(3), 379–386 (2007)
46. A. Ortlieb, M. Bouri, R. Baud, H. Bleuler, An assistive lower limb exoskeleton for people with neurological gait disorders, in *2017 International Conference on Rehabilitation Robotics (ICORR)* (2017), pp. 441–446
47. S.O. Schrade, K. Dätwyler, M. Stücheli, K. Studer, D.A. Türk, M. Meboldt, R. Gassert, O. Lambercy, Development of VariLeg, an exoskeleton with variable stiffness actuation: first results and user evaluation from the CYBATHLON 2016 Olivier Lambercy; Roger Gassert. J. NeuroEng. Rehabil. **15**(1), 1–18 (2018)
48. N. Hogan, Impedance control: an approach to manipulation, in *1984 American Control Conference* (1984), pp. 304–313

49. E.S. Barjuei, S. Toxiri, G.A. Medrano-Cerda, D.G. Caldwell, J. Ortiz, Bond graph modeling of an exoskeleton actuator, in *2018 10th Computer Science and Electronic Engineering Conference, CEEC 2018 - Proceedings* (2019), pp. 101–106
50. F.R.O. Andres, A. Lopez-Delis, A.F. da Rocha, *Upper and Lower Extremity Exoskeletons* (Elsevier, Amsterdam, 2018)
51. Z. Li, Z. Yin, Position tracking control of mass spring damper system with time-varying coefficients, in *Proceedings of the 29th Chinese Control and Decision Conference, CCDC 2017* (2017), pp. 4994–4998
52. A.A. Nikooyan, A.A. Zadpoor, Mass-spring-damper modelling of the human body to study running and hopping-an overview. Proc. Inst. Mech. Eng H J. Eng. Med. **225**(12), 1121–1135 (2011)
53. C. Bayón, O. Ramírez, F. Mollà, J. Serrano, M. Del Castillo, J. Belda-Lois, R. Poveda, R. Raya, T. Martín Lorenzo, I. Martínez Caballero, S. Lerma Lara, C. Cifuentes, A. Frizera, E. Rocon, CPWalker, robotic platform for gait rehabilitation and training in patients with cerebral palsy, in *2016 IEEE International Conference on Robotics and Automation (ICRA)* (2015), pp. 3736–3741
54. A.C. Villa-Parra, D. Delisle-Rodriguez, T. Botelho, J.J.V. Mayor, A.L. Delis, R. Carelli, A. Frizera Neto, T.F. Bastos, Control of a robotic knee exoskeleton for assistance and rehabilitation based on motion intention from sEMG. Res. Biomed. Eng. **34**(3), 198–210 (2018)
55. M.D. Sánchez Manchola, L.J. Arciniegas Mayag, M. Munera, C.A. Garcia, Impedance-based backdrivability recovery of a lower-limb exoskeleton for knee rehabilitation, in *4th IEEE Colombian Conference on Automatic Control: Automatic Control as Key Support of Industrial Productivity, CCAC 2019 - Proceedings* (2019), pp. 1–6
56. J.B. Webster, B.J. Darter, Principles of normal and pathologic gait, in *Atlas of Orthoses and Assistive Devices*, chap. 4, 5th edn. (Elsevier, Amsterdam, 2019), pp. 49–62.e1
57. T. Roskilly, R. Mikalsen, Closed-loop stability, in *Marine Systems Identification, Modeling and Control* (Elsevier, Amsterdam, 2015), pp. 97–122
58. K. Wen, D. Necsulescu, J. Sasiadek, Haptic force control based on impedance/admittance control. IFAC Proc. Vol. **38**(1), 427–432 (2005)
59. A. Fortin-Coté, P. Cardou, C. Gosselin, An admittance control scheme for haptic interfaces based on cable-driven parallel mechanisms, in *Proceedings - IEEE International Conference on Robotics and Automation* (2014), pp. 819–825
60. M. Bortole, A. Del Ama, E. Rocon, J.C. Moreno, F. Brunetti, J.L. Pons, A robotic exoskeleton for overground gait rehabilitation, in *Proceedings - IEEE International Conference on Robotics and Automation* (2013), pp. 3356–3361
61. S.K. Banala, S.H. Kim, S.K. Agrawal, J.P. Scholz, Robot assisted gait training with active leg exoskeleton (ALEX), in *Proceedings of the 2nd Biennial IEEE/RAS-EMBS International Conference on Biomedical Robotics and Biomechatronics, BioRob 2008*, vol. 17 (2008), pp. 653–658